Physiology and Pharmacology 30 (2026) 81-97
Experimental Research Article

An optimized sondell decellularization method for sciatic nerve graft

Hananeh Ahmadnia[1], Muhammad Parsa Pashazadeh[2,3], Ali Moradi[4,5], Naser Mahdavi-Shahri[1], Morteza Behnam-Rassouli[1*], Esmail Riahi[2,3*]

1. Department of Biology, Faculty of Science, Ferdowsi University of Mashhad, Mashhad, Iran
2. Electrophysiology Research Center, Neuroscience Institute, Tehran University of Medical Sciences, Tehran, Iran
3. Department of Physiology, School of Medicine, Tehran University of Medical Sciences, Tehran, Iran
4. Orthopedic Research Center, Mashhad University of Medical Sciences, Mashhad, Iran
5. The Clinical Research Development Unit, Ghaem Hospital, Mashhad University of Medical Sciences, Mashhad, Iran

ABSTRACT

Introduction: In the realm of nerve injury repair, acellularized nerve grafts (ANGs) are gaining recognition as a promising tissue engineering approach, offering better regeneration outcomes compared to traditional nerve conduits. This study, conducted on rat and chicken sciatic nerves (R-ANGs and C-ANGs, respectively), seeks to explore an optimized nerve decellularization technique that achieves effective decellularization while preserving the extracellular matrix (ECM) integrity.

Methods: The Sondell decellularization (SD) protocol was evaluated against an optimized Sondell decellularization (OSD) method improved by DNase treatment and extra-washing with ultrapure water, and then MTT, DNA quantification, mechanical tensile, and histological evaluations were performed.

Results: Results showed that both R-ANGs and C-ANGs prepared by the OSD method had better biocompatibility, measured by MTT, than those prepared by the SD ($p < 0.001$). DNA quantification of samples obtained from the OSD method showed an improved elimination of residual DNA fragments ($p < 0.0001$). Mechanical tensile test also revealed a higher Young's modulus of the OSD grafts ($p < 0.05$). Histological studies, including hematoxylin and eosin, Masson's trichrome, Luxol fast blue, DAPI, and scanning electron microscopy (FESEM), confirmed that the OSD was superior to the SD in preserving ECM while equally removing cell nuclei and myelinated fibers.

Conclusion: The OSD protocol yielded promising results for more reliable in vivo trials, as in vitro tests revealed better preservation of ECM components compared to the SD method. Notably, the OSD provided higher biocompatibility and improved viscoelastic integrity of the R-ANGs and C-ANGs.

Keywords:
Peripheral nerve injuries
Decellularized extracellular matrix
Scaffold
Sciatic Nerve

* Corresponding authors: Morteza Behnam-Rassouli, Behnam@um.ac.ir
Esmail Riahi, riahi@tums.ac.ir

Received 23 September 2025; Revised from 18 October 2025; Accepted 26 October 2025

Citation: Ahmadnia H, Pashazadeh MP, Moradi A, Mahdavi-Shahri N, Behnam-Rassouli M, Riahi E. An optimized sondell decellularization method for sciatic nerve graft. Physiology and Pharmacology 2026; 30: 81-97.

Introduction

Peripheral nerve injuries are relatively common and can result in a wide spectrum of functional and physiological impairments, depending on the nature and severity of the trauma. Wallerian degeneration is a pivotal process that happens after peripheral nerve injury, involving the disintegration of axons and the apoptosis of Schwann cells and fibroblasts (Wang et al., 2022). It is followed by regenerative processes, in which both the axon and neuronal soma initiate a coordinated response involving transcriptional reprogramming. This includes the downregulation of genes associated with synaptic activity and conduction, and the upregulation of regeneration-associated genes (He and Jin 2016), thereby shifting the neuron into a pro-regenerative state (Allodi et al., 2012). These changes are driven by chemical cues from the injured axon, including calcium influx and cytoskeletal disruption, which propagate retrograde signals to the cell body, or soma. If regeneration is feasible, the distal axon forms a growth cone, supported by localized mRNA translation and protein synthesis (Terenzio et al., 2018). The distal nerve environment is critical for successful repair, with Wallerian degeneration, myelin breakdown, and efficient debris clearance serving as prerequisites for functional recovery (Arthur-Farraj et al., 2012). Factors such as age, sex, and underlying health conditions significantly influence the regenerative capacity of the peripheral nerves (Kuffler and Foy 2020). However, timely and appropriate intervention is critical to improving clinical outcomes (Alvites et al., 2018).

Without intervention, prolonged peripheral nerve recovery may compromise regenerative outcomes, potentially leading to muscle atrophy or permanent functional deficits (Yang et al., 2020). A range of therapeutic strategies has been developed, including surgical repair, neural scaffold transplantation, neuroprotective pharmacological agents, growth factors, and stem cell-based therapies (Faroni et al., 2015). Surgical repair remains the most commonly adopted approach, with direct end-to-end suturing typically reserved for short nerve gaps (<1 cm) (Vijayavenkataraman 2020). For defects larger than 3 cm, autologous nerve grafts, commonly harvested from the sural or femoral nerves, are considered the gold standard (Hussain et al., 2020). Due to the limited availability of autografts, the exploration of allogeneic and xenogeneic nerve sources has expanded the repertoire of grafting options, with promising implications for clinical translation (Zaminy et al., 2021). Among these, decellularized nerve grafts have emerged as a leading candidate, owing to their ability to closely mimic the native nerve architecture (Sun et al., 2018). Decellularized nerves maintain a well-preserved ECM, which is crucial for promoting axonal guidance and the regeneration of peripheral nerves. Decellularized grafts are processed to eliminate immunogenic components such as cellular debris, myelin, and axons while preserving the tubular structure of the neural basement membrane. Therefore, it supports axonal guidance, cellular migration, and neovascularization (Hillebrandt et al., 2019). Various decellularization techniques have been employed to optimize graft biocompatibility and structural integrity, including irradiation, repeated freeze–thaw cycles, and detergent-based protocols. In the present study, we developed an optimized decellularization protocol based on the standard Sondell method and systematically compared it through both qualitative and quantitative analyses. The classical Sondell method utilizes Triton X-100 and sodium deoxycholate (Sondell et al., 1998), whereas our optimized protocol includes repetitive extra-washing with ultrapure water (UPW) and an enzymatic DNA removal stage using DNase. Measuring biocompatibility, mechanical tolerance, DNA content, and histological characteristics, we examined how each protocol influences cellular clearance and structural preservation within sciatic nerve tissues. Our findings will aid in selecting the most effective decellularization strategy for subsequent in vivo applications. The Sondell decellularization method, which relies exclusively on detergents such as Triton X-100 and sodium deoxycholate, has been widely applied for peripheral nerve scaffolds but presents several limitations. Due to the absence of an enzymatic digestion step, residual cellular and nuclear remnants may persist within the tissue, potentially contributing to increased immunogenicity (Hudson et al., 2004). In addition, insufficient washing between detergent cycles may leave residual detergents that can interfere with ECM integrity and cellular biocompatibility (Crapo et al., 2011; Gilbert et al., 2006). Furthermore, the exposure to strong detergents can partially degrade ECM components and alter the three-dimensional architecture, which may reduce mechanical performance and tensile strength compared with native nerve tissue (El Soury et al., 2021). To overcome these drawbacks, we

optimized Sondell's protocol and included an enzymatic digestion step to reduce immunotoxicity, extensive washing with UPW to remove detergents and cellular debris, and UV crosslinking to enhance ECM stability and mechanical integrity.

Material and Methods

Isolation and Harvesting of Nerve

All experimental procedures were approved by the Ethics Committee of Ferdowsi University of Mashhad (IR.UM.REC.1402.135) and the Ethics Committee of Tehran University of Medical Sciences (IR.TUMS.AEC.1402.151). Animals were housed under controlled conditions: temperature, 22 ± 2 °C; relative humidity, 60 ± 5%; and a 12-h light/dark cycle, with ad libitum access to standard laboratory chow and tap water. Wistar male and female rats were euthanized under deep general anesthesia (Ketamine 80 mg/kg and Xylazine 20 mg/kg), the thigh muscles were pulled away, and the sciatic nerves were exposed on both sides. Next, the entire length of the nerve was excised from the sciatic hole area to the trifurcation point. Additionally, sciatic nerves were harvested from freshly euthanized adult chickens under sterile conditions. After meticulous removal of the surrounding muscle and connective tissue, the nerves were dissected from the region distal to the sciatic notch. All isolated nerves were cleaned of residual soft tissue and sectioned into 20 mm segments. These segments were subsequently subjected to decellularization, yielding acellular nerve grafts (ANGs) for further analysis.

Decellularization of Nerve Grafts

Sciatic nerve fragments were decellularized using both the standard and an optimized protocol based on the method described by Sondell et al. (1998). In the standard Sondell decellularization (SD) protocol, nerve segments were sequentially incubated in distilled water for 7 h, 3% Triton X-100 (Sigma, USA) for 12 h, and 4% sodium deoxycholate (Sigma, USA) for 24 h, all at room temperature (RT) under constant agitation (25 rpm). This cycle was repeated once, after which the samples were rinsed with distilled water and stored in phosphate-buffered saline (PBS, pH 7.2) at 4 °C until further use (Sondell et al., 1998). In the optimized Sondell decellularization (OSD) protocol, nerve fragments were incubated in distilled water for 12 h, followed by 3% Triton X-100 for 12 h, and 4% sodium deoxycholate for 24 h. Between each step, samples were rinsed with UPW (Merck, Germany) for 15 min. This cycle was repeated once. Subsequently, each nerve sample was incubated with 10 µl DNase-I (SinaClon, Iran) in 1 ml saline for 12 h at 37 °C. Final rinsing was performed multiple times using UPW. All steps were conducted under mild rotational agitation (25 rpm). For sterilization, the decellularized grafts were washed three times for 15 min in PBS containing penicillin/streptomycin (100 µg/ml) and amphotericin B (50 µl) under gentle circular motion. The grafts were then transferred to sterile Petri dishes and immersed in 70% ethanol for 15 min. To enhance their physical integrity and improve suture tolerance during transplantation, the grafts were dried to remove residual ethanol and then exposed to ultraviolet (UV) light for 40 minutes (20 minutes per side) to induce physical cross-linking.

Cytotoxicity Analysis of the Acellular Nerve Grafts

A cytotoxicity assay was performed to examine the level of residual detergents in R-ANGs and C-ANGs. Natural nerve fragments (R-NNFs and C-NNFs; considered as controls), R-ANGs, and C-ANGs (~5 mm each) prepared using SD and OSD protocols were placed into a suspension of rat adipose-derived stem cells (ADSCs; 10,000 cells, 10 µl per well; GenIran, Iran) cultured on a 96-well plate (n = 3 with three repeats) containing Dulbecco's Modified Eagle Medium (DMEM; Gibco, USA) with 10% Fetal Bovine Serum (FBS; Gibco, USA), and incubated at 37°C in 5% CO2 under saturated humidity. The cytotoxicity of each sample was determined by measuring the optical density (OD) of 3-(4,5-dimethylthiazol-2-yl)-2,5-diphenyltetrazolium bromide (MTT; Merck, Germany) at 24 and 48 h. Briefly, 20 µl MTT reagent (5 mg/ml) was added to each well in the dark room and the samples were incubated at 37 °C for 4 h. Finally, 200 µl of dimethyl sulfoxide (DMSO; Sigma, USA) was added per well, and light absorbance of the colored Formazan products was measured at the wavelength of 630 nm using an ELISA reader (ELx 800; BioTek, USA).

DNA Quantification

To quantify residual DNA content, R-NNFs, C-NNFs, R-ANGs, and C-ANGs were subjected to papain digestion (n = 4 samples per group, with three repeats). Briefly, each sample was incubated overnight in 1 ml

of digestion buffer containing L-cysteine (0.01 M), Na_2EDTA (0.01 M), and papain (0.125 mg/ml) in sodium phosphate buffer (0.1 M), at 65 °C under intermittent agitation at 40 rpm in a shaker incubator to ensure complete homogenization and accurate DNA extraction. Following digestion, insoluble debris was precipitated, and the supernatant was collected for DNA analysis using Hoechst 33258 (0.1 ml of 1 µg/ml in TEN buffer). Serial dilutions of calf thymus DNA (Sigma, USA) were used as the standard. Fluorescence intensity was measured at excitation/emission wavelengths of 355/460 nm using a microplate reader (FLUOstar OPTIMA; BMG LABTECH, Germany), as described by (Moradi et al., 2016).

Mechanical Testing

The mechanical strength of the R-NNFs, C-NNFs, R-ANGs, and C-ANGs (SD and OSD protocols, with and without cross-linking) was measured by a tensile test. The samples (~10 mm; n = 3 per group) were loaded onto a Universal Testing Machine (SANTAM-STM20, Tehran, Iran), oriented with their length along the direction of tension, and kept moist by applying PBS during the test. They were attached at both ends to the tensile tester, and each test was run at a constant rate of 6 mm/min at RT to complete tensile failure. The force-extension diagram was recorded for each sample, and Young's modulus was calculated.

Histological Evaluation of the Nerve Grafts

To assess the preservation of key extracellular matrix (ECM) components following decellularization, histological analyses were performed on R-NNFs, C-NNFs, R-ANGs, and C-ANGs (n = 2 samples per group). Samples were fixed in 10% neutral-buffered formalin, dehydrated through a graded ethanol series, embedded in paraffin, sectioned at a thickness of 5 µm using a microtome, and mounted on glass slides. For morphological and ECM characterization, sections were stained with hematoxylin and eosin (H&E) to assess general tissue architecture, Masson's trichrome (MT) to visualize collagen fibers, and Luxol fast blue (LFB) to detect residual myelin. Stained slides were examined under a light microscope (Olympus, Japan). To evaluate the efficacy of decellularization and detect residual nuclear material, selected sections were fluorescently stained with 4′,6-diamidino-2-phenylindole (DAPI) and imaged using fluorescence microscopy. Ultrastructural features were further examined via field-emission scanning electron microscopy (FESEM). Samples were fixed in 2.5% glutaraldehyde, thoroughly rinsed to remove fixative residues, and then freeze-dried for 24 hours (Pishtaz Engineering Co.). Lyophilized specimens were sputter-coated with gold and visualized using a FESEM system (LMU TESCAN BRNO Mira3).

Statistical Analysis

Data are presented as Mean ± standard error of mean (SEM). For each comparison, the normal distribution of the data was first checked by the Shapiro-Wilk test. Parametric statistical tests were used when the data passed the normality test; otherwise, nonparametric equivalents were used. Outliers were found by the ROUT test with Q set at 1%. The two-way repeated measures analysis of variance (ANOVA) and Bonferroni post hoc were used for analyzing changes that happened over time in different groups. The one-way ANOVA and the Tukey post-hoc tests (or Kruskal-Wallis followed by Dunn's tests as nonparametric alternatives) were used to determine significant differences between the groups. The GraphPad Prism 10 software was used for all statistical analyses and for plotting the graphs. A two-tailed $p < 0.05$ was considered statistically significant.

Results

Biocompatibility Evaluation

Residual detergents entrapped within acellular nerve scaffolds can induce cytotoxic effects. To evaluate this, the cell viability and proliferation of ADSCs were assessed using the MTT assay at 24 and 48 h post-seeding. For R-ANGs, two-way ANOVA revealed significant effects of time [$F(1, 24) = 21878$, $p < 0.0001$], treatment [$F(2, 24) = 83.54$, $p < 0.0001$], and their interaction [$F(2, 24) = 5.60$, $p = 0.01$]. Tukey's post hoc analysis showed a significant reduction in cell viability and proliferation in R-ANGs processed via the SD protocol compared to R-NNFs ($p < 0.0001$) at both time points. In contrast, no significant difference was observed between R-NNFs and R-ANGs processed via the OSD protocol ($p = 0.32$ and $p = 0.06$ at 24 and 48 h, respectively). A significant improvement in cell viability was observed in R-ANGs treated with the OSD protocol compared to those treated with the SD ($p < 0.0001$), confirming the efficacy of UPW washing in removing cytotoxic detergent res-

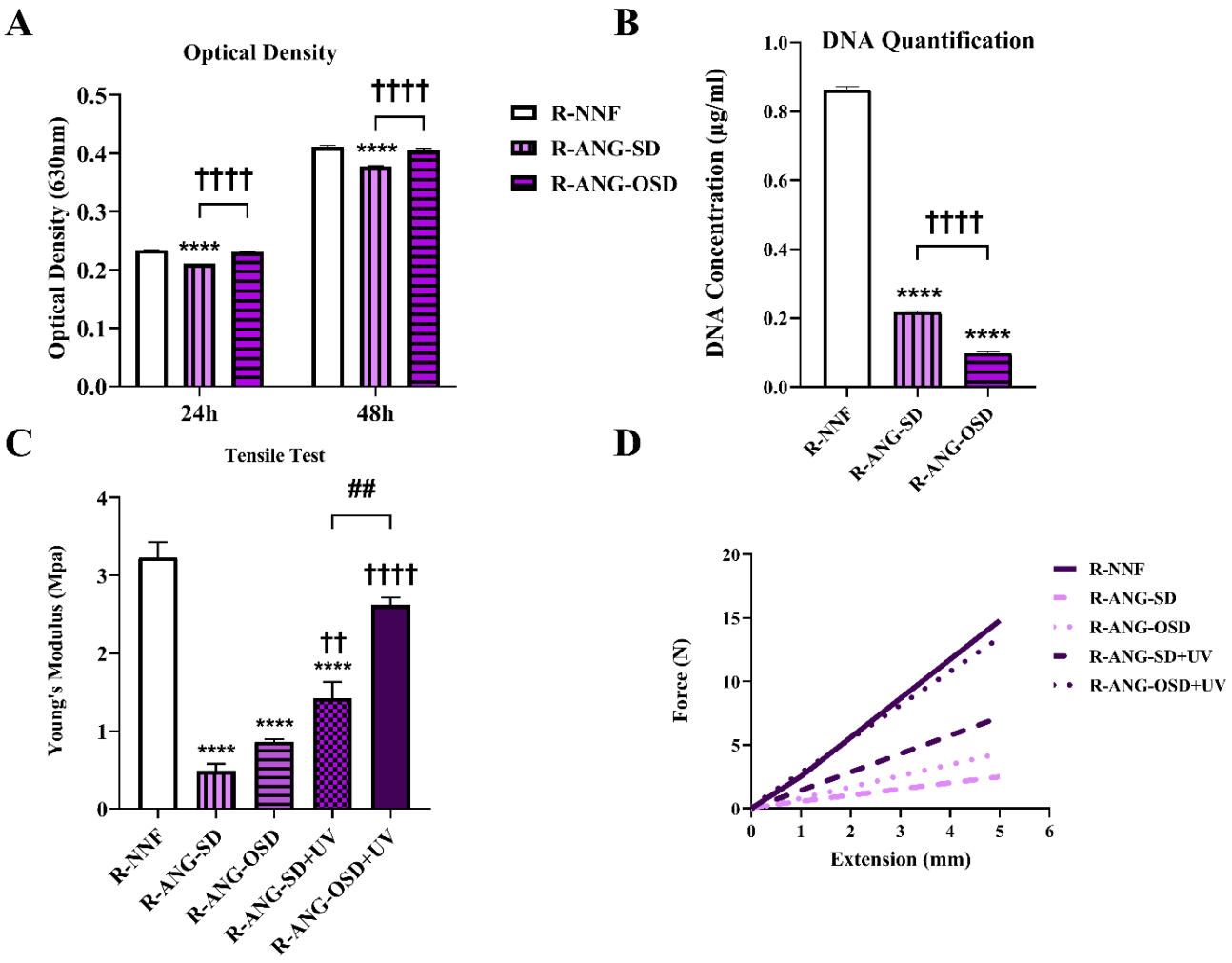

FIGURE 1. R-ANGs Cytotoxicity (A), DNA Content (B), and Mechanical Testing (C and D). A: The effects of R-ANGs prepared by SD and OSD protocols on ADSCs viability were evaluated using an MTT assay after 24 and 48 h. The experiment was conducted at least three times. $^{****}p < 0.0001$ compared with the R-NNFs group, $^{††††}p < 0.0001$. Data are presented as the mean ± SEM, n = 9. B: The concentration of total DNA in R-ANGs prepared by SD and OSD protocols was evaluated using the Hoechst 33258 assay. The experiment was conducted at least three times. $^{****}p < 0.0001$ compared with the R-NNFs group, $^{††††}p < 0.0001$. Data are presented as the mean ± SEM, n = 12. C: The mechanical strength of the R-ANGs prepared by the SD and OSD protocols with and without UV crosslinking. $^{****}p < 0.0001$ compared with the R-NNFs group, $^{††}p < 0.01$, $^{††††}p < 0.0001$ compared with their respective group without crosslinking, $^{##}p < 0.01$. Data are presented as the mean ± SEM, n = 3. D: Stress-Extension diagrams of the R-NNFs and R-ANGs prepared by SD and OSD protocols with and without cross-linking by UV.

idues (Fig. 1A). Similarly, for C-ANGs, the two-way ANOVA indicated significant effects of time [F(1, 24) = 21925, $p < 0.0001$] and treatment [F(2, 24) = 98.30, $p < 0.0001$], with no significant interaction [F(2, 24) = 1.25, $p = 0.30$]. Tukey's tests showed significantly reduced ADSC viability in C-ANGs processed via the SD protocol compared to C-NNFs ($p < 0.0001$) at both time points. However, no significant difference was found between C-NNFs and C-ANGs treated with the OSD protocol ($p = 0.06$ and $p = 0.22$ at 24 and 48 h, respectively). Notably, C-ANGs processed via the OSD exhibited significantly higher cell viability than those treated with the SD ($p < 0.001$ at both time points), further supporting the role of UPW in mitigating detergent-induced cytotoxicity (Fig. 2A).

DNA Content

Effective removal of DNA remnants is essential to minimize immunogenicity and reduce the risk of graft rejection. To this end, R-ANGs and C-ANGs were treated with DNase to eliminate residual nucleic acids. DNA concentration was 0.86 µg/ml in R-NNFs, 0.21 µg/ml in SD R-ANGs, and 0.09 µg/ml in OSD R-ANGs. One-way ANOVA [F(2, 33) = 4871, $p < 0.0001$] followed

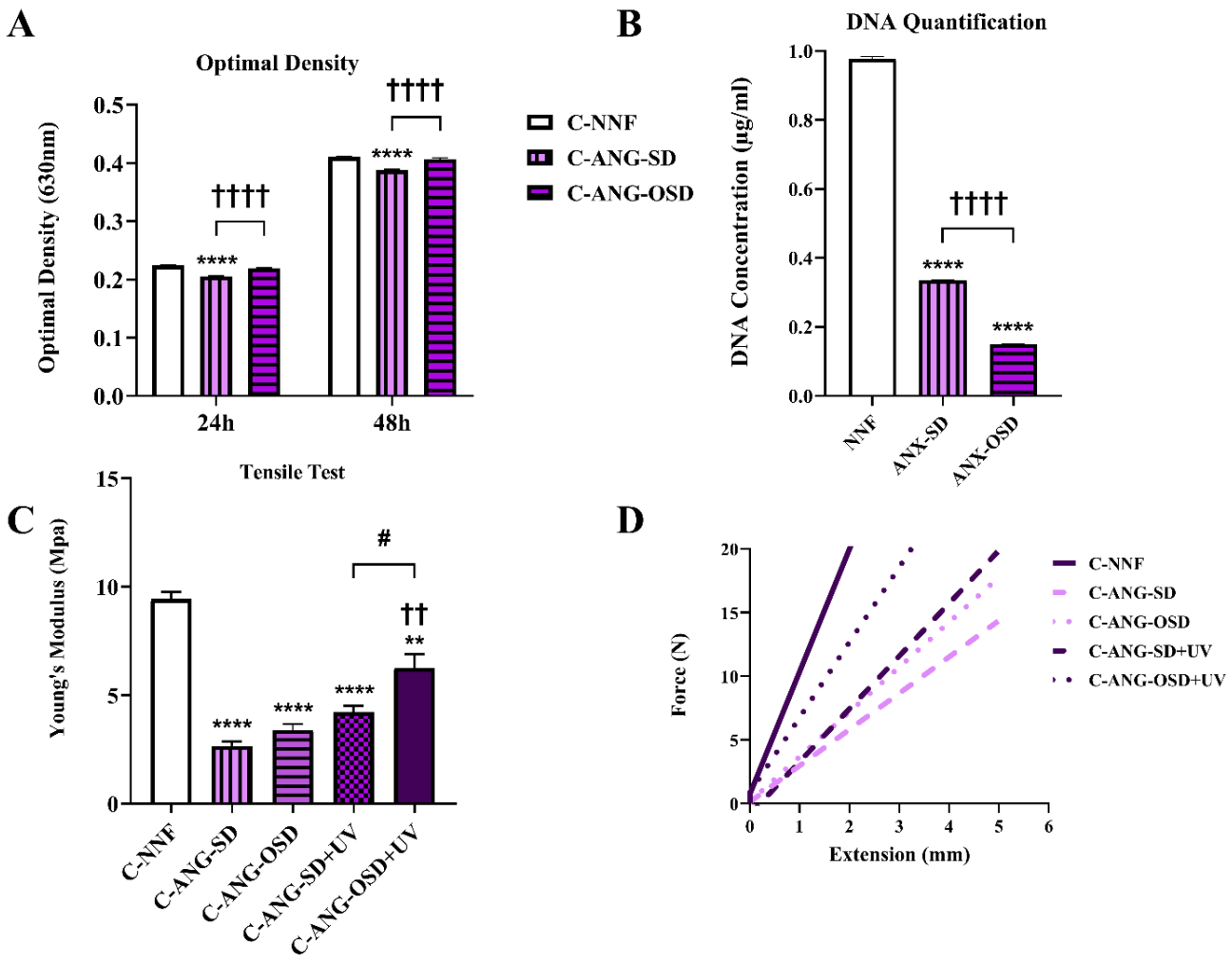

FIGURE 2. C-ANGs Cytotoxicity (A), DNA Content (B), and Mechanical Testing (C and D). A: The effects of C-ANGs prepared by SD and OSD protocols on ADSCs viability were evaluated using an MTT assay after 24 and 48 h. The experiment was conducted at least three times. $^{****}p < 0.0001$ compared with the C-NNFs group, $^{††††}p < 0.0001$. Data are presented as the mean ± SEM, n = 9. B: The concentration of total DNA in C-ANGs prepared by SD and OSD protocols was evaluated using the Hoechst 33258 assay. The experiment was conducted at least three times. $^{****}p < 0.0001$ compared with the C-NNFs group, $^{††††}p < 0.0001$. Data are presented as the mean ± SEM, n = 12. C: The mechanical strength of the C-ANGs prepared by the SD and OSD protocols with and without UV cross-linking. $^{**}p < 0.01$, $^{****}p < 0.0001$ compared with the C-NNFs group, $^{††}p < 0.01$ compared with the OSD group, $^{#}p < 0.05$. Data are presented as the mean ± SEM, n = 3. D: Stress-Extension diagrams of the C-NNFs and C-ANGs prepared by SD and OSD protocols with and without cross-linking by UV.

by Tukey's post hoc analysis confirmed statistically significant differences among all groups ($p < 0.0001$; Fig. 1B), indicating enhanced DNA removal with the OSD protocol. DNA concentration was 0.97 µg/ml in C-NNFs, 0.33 µg/ml in SD C-ANGs, and 0.14 µg/ml in OSD C-ANGs. One-way ANOVA [$F(2, 33) = 10959$, $p < 0.0001$] and Tukey's tests again revealed significant differences between all groups ($p < 0.0001$; Fig. 2B), demonstrating the superior efficacy of the OSD protocol in reducing residual DNA content.

Mechanical Testing

To evaluate the viscoelastic integrity of the grafts, tensile testing was performed to measure Young's modulus as an indicator of elasticity. In this experiment, we further evaluated the effect of UV irradiation on the integrity of nerve grafts. One-way ANOVA [$F(4, 10) = 66.80$, $p < 0.0001$] followed by Tukey's post hoc analysis revealed a significant reduction ($p < 0.0001$) in Young's modulus in both SD and OSD R-ANGs compared to R-NNFs, indicating severe damage to the scaffolds (Fig. 1C, 1D). No significant difference was observed be-

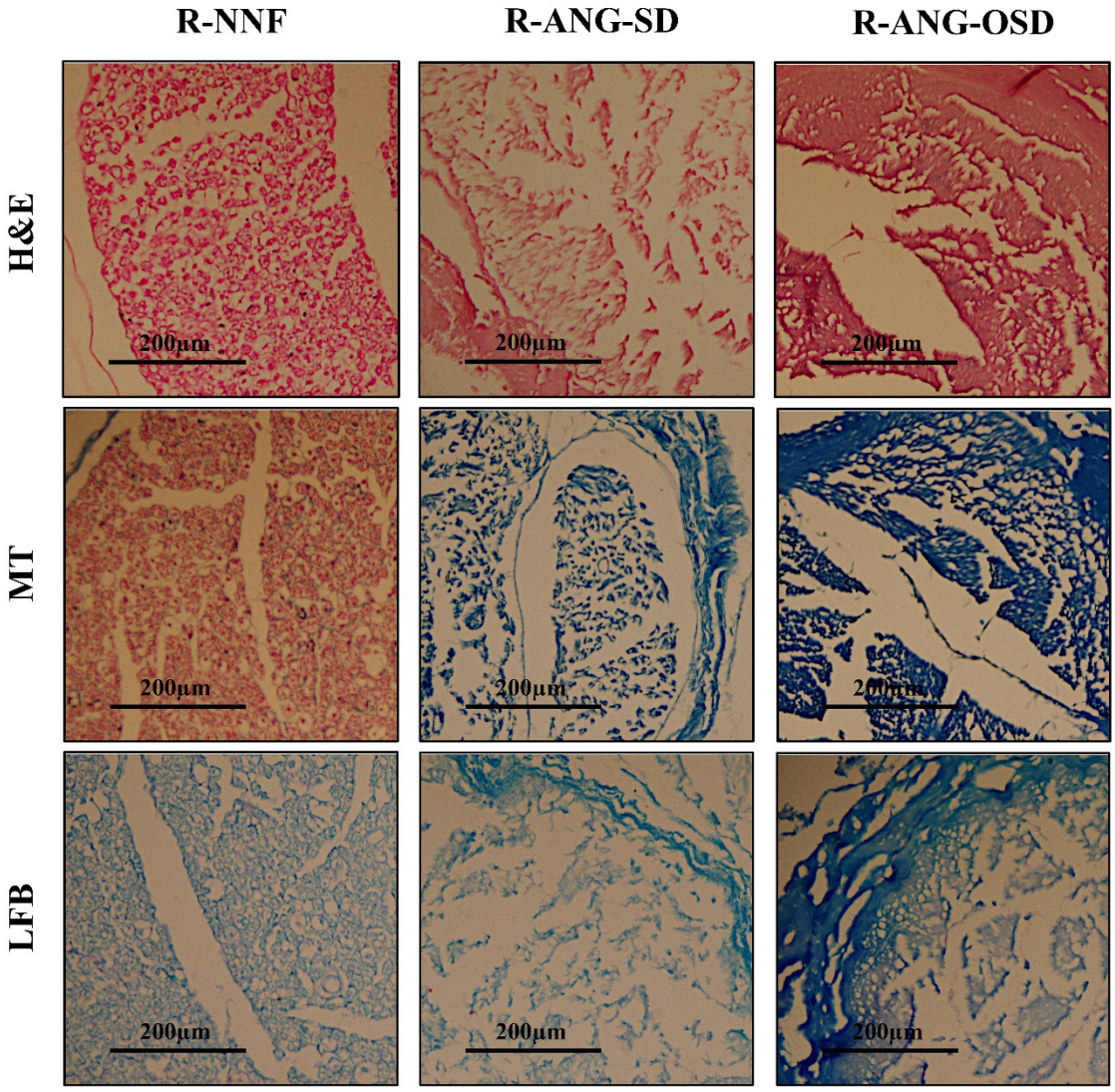

FIGURE 3. Histological Sections of R-NNFs and R-ANGs. Cross-sectional images of R-NNFs and R-ANGs were stained using hematoxylin and eosin (H&E), Masson's Trichrome (MT), and Luxol fast blue (LFB). H&E staining demonstrated Schwann cell nuclei and the myelin sheaths in the R-NNFs; in contrast, a high degree of cellular removal with minimal disruption was observed in the SD and OSD protocols. However, it appears that the OSD protocol preserves ECM morphology more effectively than the SD protocol. MT staining of the R-NNFs displays predominant pink staining of cellular and myelin-rich regions, with collagen fibers barely visible. The R-ANGs show intense blue staining of collagen fibers, indicating effective removal of cellular components. The SD protocol preserves a uniform collagen network, while the OSD protocol yields more compact and distinctly organized collagen bundles. LFB staining revealed that almost all the R-ANGs were efficiently removed from myelin sheaths in the SD and OSD protocols, whose presence was evident in the R-NNFs. Arrows indicate the nuclei—scale bars: 200 µm.

tween SD and OSD R-ANGs ($p = 0.39$). However, UV irradiation significantly enhanced the elasticity of both R-ANG groups ($p < 0.01$ for SD R-ANGs; $p < 0.0001$ for OSD R-ANGs). Notably, the improvement in the OSD R-ANGs was significantly greater than that in the SD R-ANGs ($p < 0.01$), resulting in no significant difference in elasticity between R-NNFs and UV-treated OSD R-ANGs ($p = 0.07$).

Similarly, one-way ANOVA [$F(4, 10) = 50.93$, $p < 0.0001$] and Tukey's tests ($p < 0.0001$) demonstrated a significant decrease in Young's modulus in both SD and OSD C-ANGs compared to the C-NNFs (Fig. 2C, 2D). No significant difference was found between SD and OSD C-ANGs ($p = 0.66$). UV irradiation improved elasticity in both groups; however, the enhancement was statistically significant only in the OSD C-ANGs ($p <$

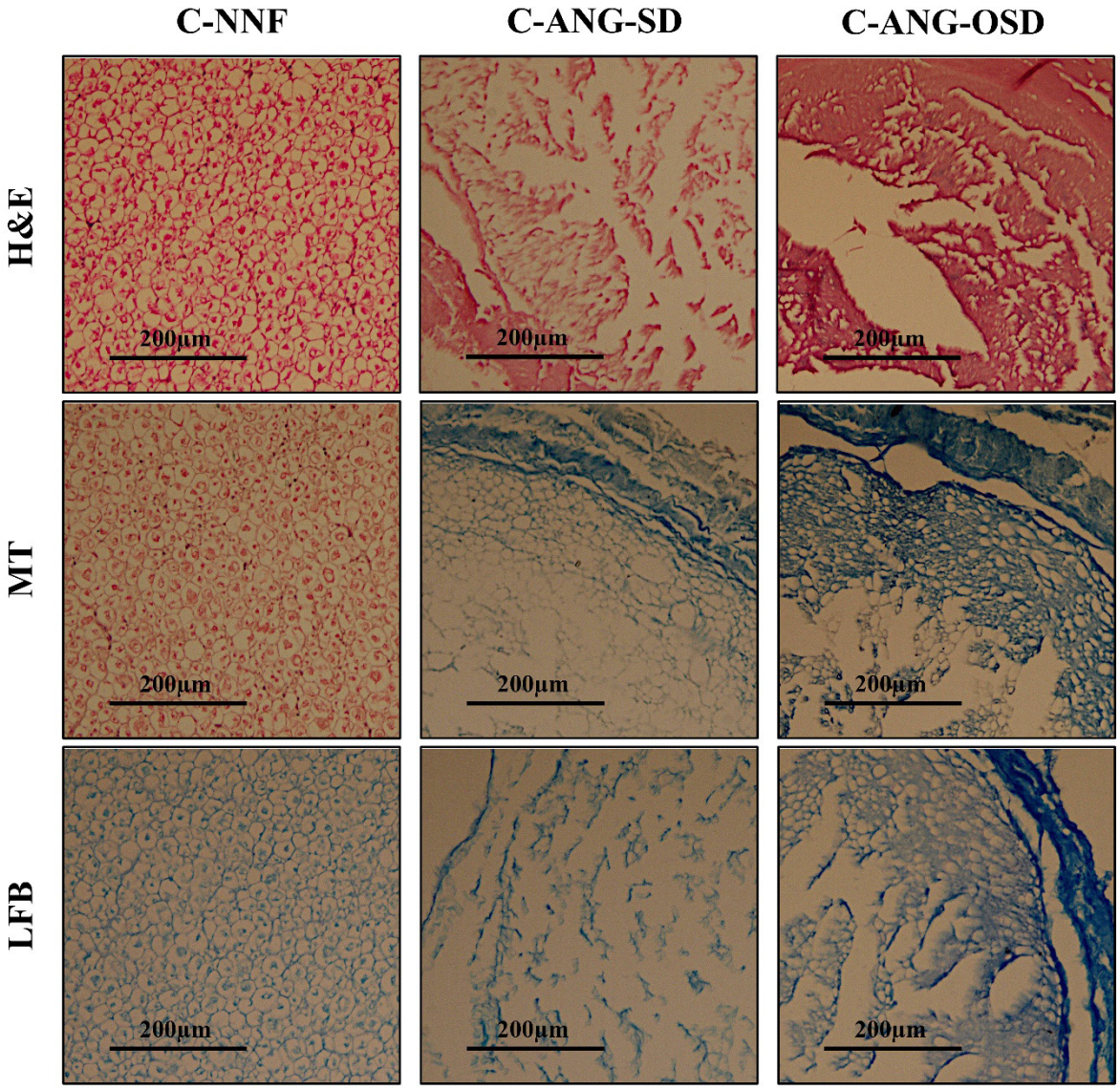

FIGURE 4. Histological Sections of C-NNFs and C-ANGs. Cross-sectional images of C-NNFs and C-ANGs were stained using hematoxylin and eosin (H&E), Masson's Trichrome (MT), and Luxol fast blue (LFB). H&E staining demonstrated Schwann cell nuclei and the myelin sheaths in the C-NNFs; in contrast, a high degree of cellular removal with minimal disruption was observed in the SD and OSD protocols. However, it appears that the OSD protocol preserves ECM morphology more effectively than the SD protocol. MT staining of the C-NNFs displays predominant pink staining of cellular and myelin-rich regions, with collagen fiber barely visible. The C-ANGs show intense blue staining of collagen fibers, indicating effective removal of cellular components. The SD protocol preserves a uniform collagen network, whereas the OSD protocol yields more compact and distinctly organized collagen bundles. LFB staining revealed that almost all the C-ANGs were efficiently removed from myelin sheaths in the SD and OSD protocols, whose presence was evident in the C-NNFs. Arrows indicate the nuclei—scale bars: 200 µm.

0.01). Moreover, the improvement in the OSD C-ANGs was significantly greater than that in the SD C-ANGs ($p < 0.05$), resulting in a significant difference in elasticity between C-NNFs and UV-treated OSD C-ANGs ($p < 0.01$). These findings highlight the mechanical benefits of UV treatment, particularly when combined with the OSD protocol, in restoring scaffold elasticity toward native tissue levels.

Histological Evaluation

Histological staining was performed after completion of the decellularization process to assess cellular clearance and preservation of the ECM. The efficacy of both the SD and OSD protocols in removing cellu-

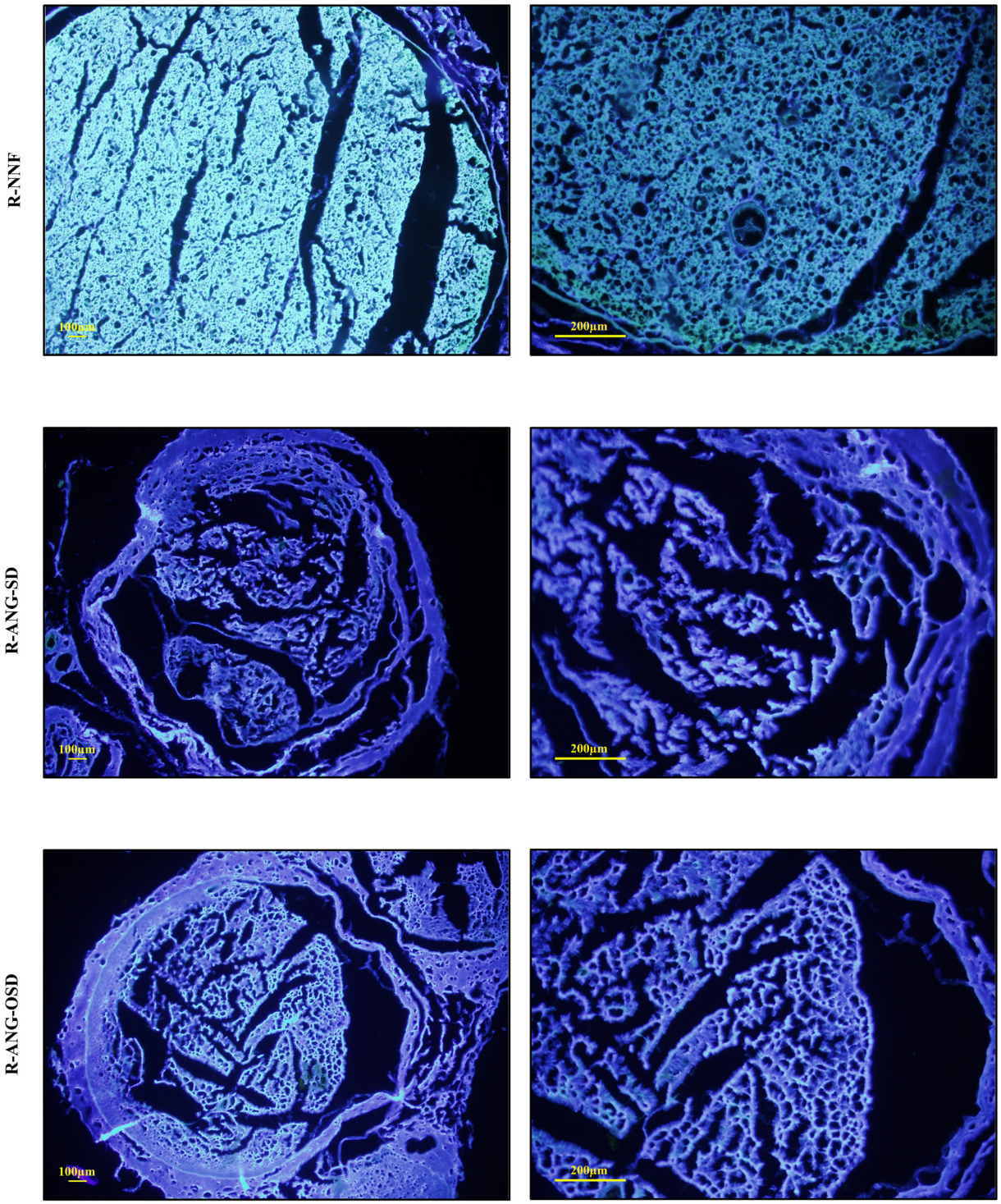

FIGURE 5. Fluorescence micrographs of 4′,6-diamidino-2-phenylindole (DAPI)-stained cross sections of R-NNFs and R-ANGs. In the native nerve (R-NNF), numerous bright and clearly defined DAPI-positive nuclei (blue) are uniformly distributed throughout the tissue, indicating the presence of intact cellular components. In contrast, both decellularized samples (R-ANG-SD and R-ANG-OSD) show the complete absence of nuclear staining, with empty cavities corresponding to the former locations of cells, confirming the efficient removal of nuclear material and cellular residues. Scale bars: 100 µm and 200 µm.

lar components was confirmed through microscopic analysis (Figs. 3 and 4). H&E staining of the R-NNFs and C-NNFs revealed dense cellularity throughout the tissue, whereas both SD and OSD protocols achieved

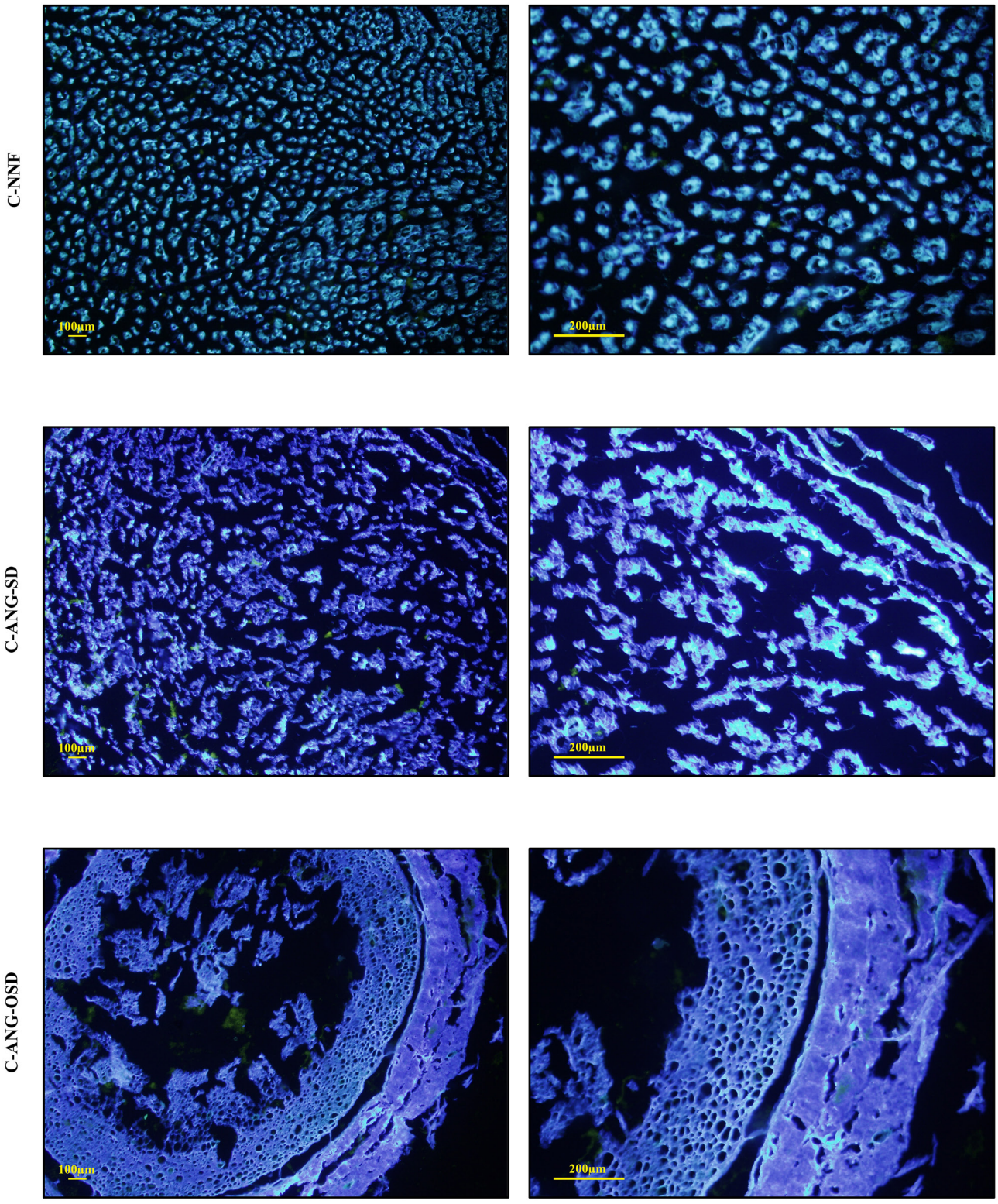

FIGURE 6. Fluorescence micrographs of 4′,6-diamidino-2-phenylindole (DAPI)-stained cross sections of C-NNFs and C-ANGs. In the native nerve (C-NNF), numerous bright and clearly defined DAPI-positive nuclei (blue) are uniformly distributed throughout the tissue, indicating the presence of intact cellular components. In contrast, both decellularized samples (C-ANG-SD and C-ANG-OSD) show the complete absence of nuclear staining, with empty cavities corresponding to the former locations of cells, confirming the efficient removal of nuclear material and cellular residues. Scale bars: 100 µm and 200 µm.

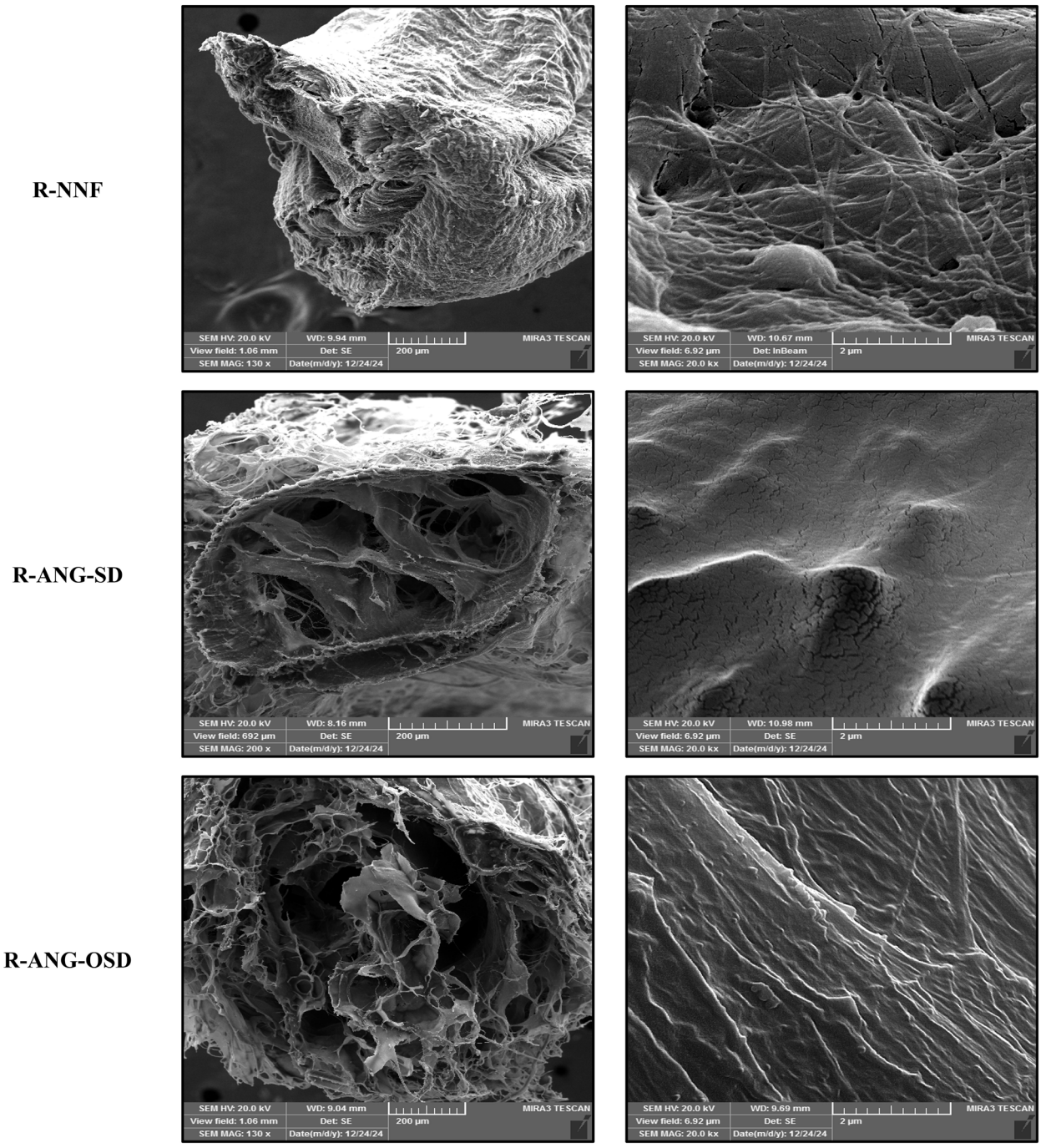

FIGURE 7. Field-emission scanning electron microscopy (FESEM) of R-NNFs and R-ANGs. The localized morphological changes, slight disruptions in the ECM, and surface irregularities were shown. At the same time, the spatial organization and three-dimensional structural integrity were preserved, and cellular contents were substantially eliminated.

substantial cellular elimination with minimal disruption of the underlying fibrous architecture. Notably, the OSD protocol induced only minor morphological alterations of the ECM compared to the R-NNFs and C-NNFs, resulting in superior preservation of the ECM components relative to the SD protocol. These findings suggest that the OSD protocol is not only effective in removing cellular debris but also in maintaining structural integrity. Masson's trichrome (MT) staining of the R-NNFs and C-NNFs revealed predominantly pink cytoplasmic

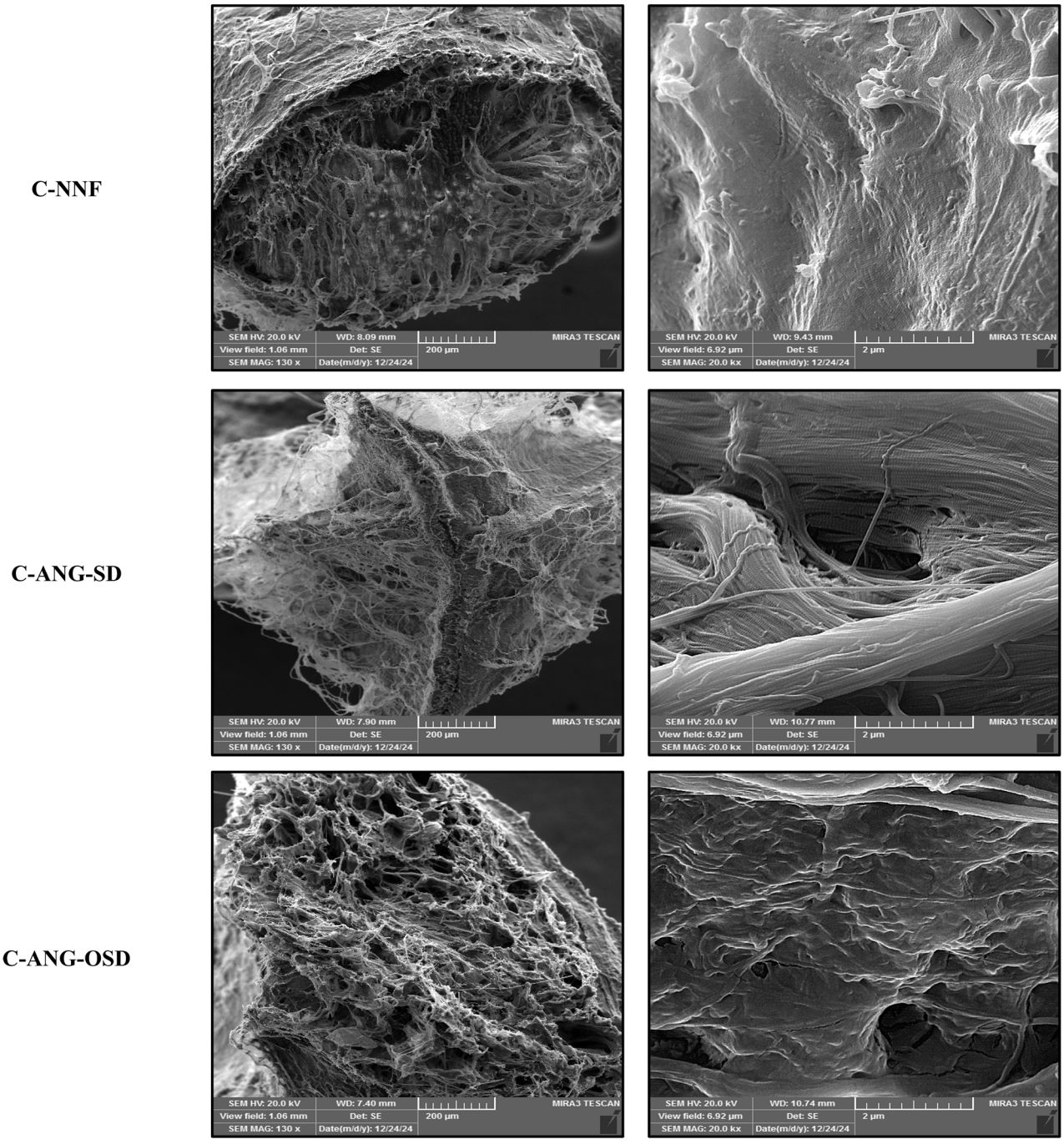

FIGURE 8. Field-emission scanning electron microscopy (FESEM) of C-NNFs and C-ANGs. The localized morphological changes, slight disruptions in the ECM, and surface irregularities were shown. At the same time, the spatial organization and three-dimensional structural integrity were preserved, and cellular contents were substantially eliminated.

regions rich in myelin, with limited visibility of blue-stained collagen fibers. This pattern reflects the high cellular and myelin content that physically and optically obscures ECM components. Following decellularization, both protocols successfully removed cellular and myelin elements, leading to enhanced visualization of collagen fibers. The SD protocol produced a moderately compact and uniform collagen network. In contrast, the OSD protocol yielded more intensely stained, well-defined, and tightly packed collagen bundles, indicative of

more effective decellularization and better ECM preservation. Luxol fast blue (LFB) staining confirmed effective myelin removal in nearly all R-ANGs and C-ANGs processed by either protocol, while myelin sheaths remained prominent in R-NNFs and C-NNFs sections. Again, the OSD protocol demonstrated superior preservation of ECM components, particularly collagen fibers (Figs. 3 and 4). To assess nuclear content, DAPI staining was performed. DAPI is a blue-fluorescent dye that binds preferentially to adenine-thymine (AT)-rich regions of DNA and is commonly used for nuclear visualization. All R-ANGs and C-ANGs processed via SD and OSD protocols showed complete loss of nuclear material, confirming successful decellularization. Microscopic observations at various magnifications revealed that the OSD protocol caused less structural damage to the ECM and was more effective in preserving its components (Figs. 5 and 6). Ultrastructural analysis using field-emission scanning electron microscopy (FESEM) further validated the structural integrity of the decellularized grafts. The three-dimensional architecture of R-ANGs and C-ANGs remained largely intact, supporting their potential for cellular infiltration and regenerative applications. Although localized morphological changes were observed, such as surface irregularities and minor ECM disruptions, these were attributed to chemical processing. Importantly, the overall spatial organization was preserved, indicating that the scaffolds retain sufficient mechanical and structural fidelity to support subsequent nerve regeneration (Figs. 7 and 8).

Discussion

Decellularized nerve grafts (R-ANGs and C-ANGs) are emerging alternatives that could replace the current gold standard, peripheral nerve autografts. They offer the advantage of being easily accessible and support the migration of Schwann cells and sprouting axons during sciatic nerve regeneration (El Soury et al., 2021; Philips et al., 2018). Since ECM molecules, such as collagen, laminin, and glycosaminoglycans, are crucial for both structural support and biochemical signaling in axonal regrowth and Schwann cell movement, decellularization techniques that effectively preserve these molecules while removing cellular and antigenic components yield increasingly better outcomes (Sridharan et al., 2015; Zilic et al., 2016). However, finding a protocol that achieves both sufficient cellular clearance and strong ECM preservation remains an ongoing challenge. Although detergent-based methods, such as the SD protocol, have been used for many years to achieve effective decellularization, this aggressive approach not only damages the ECM structure but also causes degradation of laminin and glycosaminoglycans, resulting in increased tissue stiffness (Philips et al., 2018). Additionally, detergent residues act as potent cytotoxic stressors, inhibiting cellular metabolism and preventing recellularization (Alizadeh et al., 2019).

Here, we evaluated the performance of our OSD protocol against the SD protocol. MTT assay showed that the OSD protocol outperformed the SD in terms of biocompatibility. The viability of ADSCs cultured with OSD-prepared scaffolds was significantly higher than that of cells cultured with SD scaffolds. It seems that the inclusion of additional washes with UPW in the OSD protocol has led to this improvement. These results are consistent with previous findings that additional washes improved the removal of cytotoxic detergent residues (Keane et al., 2015). Moreover, decellularized matrices appear to have higher proliferative and trophic activity when the substrate is well-rinsed and structurally intact, reinforcing our viability findings (Faroni et al., 2014; Moreno-Manzano et al., 2020).

DNA elimination is another critical factor in increasing the safety of tissue-engineered products in that it reduces the immunogenicity risks associated with allogeneic and xenogeneic grafts (Kasravi et al., 2023). Therefore, the addition of enzymatic digestion steps to detergent-based protocols is crucial for achieving safer decellularization and maintaining the functionality of the scaffolds. It has been shown that the combination of Triton X-100 with DNase, RNase, and trypsin effectively removes nuclear content while preserving the ultrastructure of endoneurial tubes and ECM components, such as collagen. Additionally, it was associated with greater cell compatibility and improved attachment and proliferation of ADSCs (Philips et al., 2018). In the present study, R-ANGs and C-ANGs from both the SD and OSD protocols proved to have significantly less DNA content than R-NNFs and C-NNFs. However, the OSD protocol was superior to the SD protocol in DNA elimination. This meets the current quantitative requirements for successful decellularization, which have been repeatedly linked to a lower immunogenic risk, including < 50 ng dsDNA/mg dry ECM, DNA fragments < 200

bp, and no visible nuclei on DAPI staining (Crapo et al., 2011; García-Gareta et al., 2020; Gilpin and Yang 2017). These decreases in DNA content are especially crucial to xenogeneic scaffolds, where antigenic remnants might trigger innate and adaptive responses that in turn cause unfavorable remodeling (Kasravi et al., 2023; Wong and Griffiths 2014).

Another event that occurs during decellularization is damage to the biophysical properties of the ECM. The use of detergents, even at low concentrations, proved to cause significant changes in the structure and composition of the ECM, ultimately affecting cell adhesion and growth (McInnes et al., 2022). However, compensatory strategies such as crosslinking by UV treatment can help restore the structural flexibility of scaffolds and increase physical strength (Ahearne and Coyle 2016). Recent advances in scaffold technology focus on optimizing crosslinking methods to strike a balance between mechanical strength and biological function. Crosslinking agents enhance the tensile properties and affect degradation rates, which are crucial for tissue integration (Liu et al., 2023). Improved scaffold properties support better performance in applications such as organ repair and regenerative medicine (Chen et al., 2023).

In this present study, the results of mechanical testing showed a significant decrease in Young's modulus after decellularization, which is related to damage to the ECM. However, crosslinking with UV radiation significantly improved the tensile strength. Additionally, the combination of the OSD protocol with UV crosslinking showed a better improvement in mechanical performance compared with the SD protocol with UV crosslinking. These results align with recent research demonstrating improvement in the structural stability of collagen scaffolds for implantation by UV radiation (Zhang et al., 2021). Collectively, these findings highlight the potential of UV crosslinking in developing durable ECM scaffolds, ultimately enhancing outcomes in tissue engineering and regenerative strategies. Recent advancements in decellularization techniques are based on preserving the ECM structure and minimizing disruption (Golebiowska et al., 2024), which can lead to improved cellular interactions after transplantation and enhanced integration and functionality of the engineered tissues (Rosadas et al., 2024).

Our histological evaluations indicated that the OSD protocol, in addition to successfully decellularizing and removing myelin, was more effective in preserving the ECM architecture, including key components such as collagen and laminin. These features are associated with Schwann cells/axon guidance in nerve scaffolds (Bae et al., 2021; Sondell et al., 1998). Results of systematic reviews of decellularized nerve grafts in rodents report that chemical protocols containing Triton X-100, deoxycholate, and SDS variants outperform purely physical methods and can support functional regeneration when the ECM microarchitecture is preserved (El Soury et al., 2021; Lovati et al., 2018). Our evaluations demonstrated that the OSD, which utilized Triton X-100, sodium deoxycholate, and DNase, as well as extra-washing with UPW and physical cross-linking via UV, effectively removed cellular content while preserving most of the ECM. As such, the benefits of the OSD protocol extend beyond improved viability and DNA reduction, encompassing better tissue integration in future clinical applications. However, it also has some limitations. For example, a comparative analysis with other nerve-tailored protocols can benchmark OSD along with UV against state-of-the-art methods. Since our study was conducted in vitro, it would be beneficial to evaluate the in vivo validation of conduction velocity and muscle reinnervation.

Conclusion

Collectively, our results position the OSD protocol plus UV crosslinking as a pragmatic route to clinically relevant nerve scaffolds that unite low cytotoxicity, low residual DNA, and near-native mechanics. These scaffolds could be a promising platform for enhancing axonal regrowth and peripheral nerve regeneration and improving functional outcomes.

Acknowledgements

This work was supported by grants from the Electrophysiology Research Center, Neuroscience Institute, Tehran University of Medical Sciences [1402-3-233-68562], School of Medicine, Tehran University of Medical Sciences [1402-3-233-68562], and the Research Council, Ferdowsi University of Mashhad [3/60798].

Conflict of interest

The authors declare that there is no conflict of interest regarding this work.

Ethics approval

All experimental procedures were approved by the Ethics Committee of Ferdowsi University of Mashhad (IR.UM.REC.1402.135) and the Ethics Committee of Tehran University of Medical Sciences (IR.TUMS.AEC.1402.151).

References

Ahearne M, Coyle A. Application of UVA-riboflavin cross-linking to enhance the mechanical properties of extracellular matrix derived hydrogels. Journal of the Mechanical Behavior of Biomedical Materials 2016; 54: 259-267. https://doi.org/10.1016/j.jmbbm.2015.09.035

Alizadeh M, Rezakhani L, Soleimannejad M, Sharifi E, Anjomshoa M, Alizadeh A. Evaluation of vacuum washing in the removal of SDS from decellularized bovine pericardium: method and device description. Heliyon 2019; 5. https://doi.org/10.1016/j.heliyon.2019.e02253

Allodi I, Udina E, Navarro X. Specificity of peripheral nerve regeneration: interactions at the axon level. Progress in Neurobiology 2012; 98: 16-37. https://doi.org/10.1016/j.pneurobio.2012.05.005

Alvites R, Rita Caseiro A, Santos Pedrosa S, Vieira Branquinho M, Ronchi G, Geuna S, et al. Peripheral nerve injury and axonotmesis: State of the art and recent advances. Cogent Medicine 2018; 5: 1466404. https://doi.org/10.1080/2331205X.2018.1466404

Arthur-Farraj P J, Latouche M, Wilton D K, Quintes S, Chabrol E, Banerjee A, et al. c-Jun reprograms Schwann cells of injured nerves to generate a repair cell essential for regeneration. Neuron 2012; 75: 633-647. https://doi.org/10.1016/j.neuron.2012.06.021

Bae J-Y, Park S Y, Shin Y H, Choi S W, Kim J K. Preparation of human decellularized peripheral nerve allograft using amphoteric detergent and nuclease. Neural Regeneration Research 2021; 16: 1890-1896. https://doi.org/10.4103/1673-5374.306091

Chen L, Wei L, Su X, Qin L, Xu Z, Huang X, et al. Preparation and characterization of biomimetic functional scaffold with gradient structure for osteochondral defect repair. Bioengineering 2023; 10: 213. https://doi.org/10.3390/bioengineering10020213

Crapo P M, Gilbert T W, Badylak S F. An overview of tissue and whole organ decellularization processes. Biomaterials 2011; 32: 3233-3243. https://doi.org/10.1016/j.biomaterials.2011.01.057

El Soury M, García-García Ó D, Moretti M, Perroteau I, Raimondo S, Lovati A B, et al. Comparison of decellularization protocols to generate peripheral nerve grafts: a study on rat sciatic nerves. International Journal of Molecular Sciences 2021; 22: 2389. https://doi.org/10.3390/ijms22052389

Faroni A, Mobasseri S A, Kingham P J, Reid A J. Peripheral nerve regeneration: experimental strategies and future perspectives. Advanced Drug Delivery Reviews 2015; 82: 160-167. https://doi.org/10.1016/j.addr.2014.11.010

Faroni A, Smith R J, Reid A J. Adipose derived stem cells and nerve regeneration. Neural Regeneration Research 2014; 9: 1341-1346. https://doi.org/10.4103/1673-5374.137585

García-Gareta E, Abduldaiem Y, Sawadkar P, Kyriakidis C, Lali F, Greco K V. Decellularised scaffolds: just a framework? Current knowledge and future directions. Journal of Tissue Engineering 2020; 11: 2041731420942903. https://doi.org/10.1177/2041731420942903

Gilbert T W, Sellaro T L, Badylak S F. Decellularization of tissues and organs. Biomaterials 2006; 27: 3675-3683. https://doi.org/10.1016/j.biomaterials.2006.02.014

Gilpin A, Yang Y. Decellularization strategies for regenerative medicine: from processing techniques to applications. Biomed Research International 2017; 2017: 9831534. https://doi.org/10.1155/2017/9831534

Golebiowska A A, Intravaia J T, Sathe V M, Kumbar S G, Nukavarapu S P. Decellularized extracellular matrix biomaterials for regenerative therapies: advances, challenges and clinical prospects. Bioactive Materials 2024; 32: 98-123. https://doi.org/10.1016/j.bioactmat.2023.09.017

He Z, Jin Y. Intrinsic control of axon regeneration. Neuron 2016; 90: 437-451. https://doi.org/10.1016/j.neuron.2016.04.022

Hillebrandt K H, Everwien H, Haep N, Keshi E, Pratschke J, Sauer I M. Strategies based on organ decellularization and recellularization. Transplant International 2019; 32: 571-585. https://doi.org/10.1111/tri.13462

Hudson T W, Zawko S, Deister C, Lundy S, Hu C Y, Lee K, et al. Optimized acellular nerve graft is immunologically tolerated and supports regeneration. Tissue Engineering 2004; 10: 1641-1651. https://doi.org/10.1089/ten.2004.10.1641

Hussain G, Wang J, Rasul A, Anwar H, Qasim M, Zafar S, et al. Current status of therapeutic approaches against peripheral nerve injuries: a detailed story from injury to recovery. International Journal of Biological Sciences 2020; 16: 116. https://doi.org/10.7150/ijbs.35653

Kasravi M, Ahmadi A, Babajani A, Mazloomnejad R, Hatamnejad M R, Shariatzadeh S, et al. Immunogenicity of decellularized extracellular matrix scaffolds: a bottleneck in

tissue engineering and regenerative medicine. Biomaterials Research 2023; 27: 10. https://doi.org/10.1186/s40824-023-00348-z

Keane T J, Swinehart I T, Badylak S F. Methods of tissue decellularization used for preparation of biologic scaffolds and in vivo relevance. Methods 2015; 84: 25-34. https://doi.org/10.1016/j.ymeth.2015.03.005

Kuffler D P, Foy C. Restoration of neurological function following peripheral nerve trauma. International Journal of Molecular Sciences 2020; 21: 1808. https://doi.org/10.3390/ijms21051808

Liu Y-Y, Blazquez J P F, Yin G-Z, Wang D-Y, Llorca J, Echeverry-Rendón M. A strategy to tailor the mechanical and degradation properties of PCL-PEG-PCL based copolymers for biomedical application. European Polymer Journal 2023; 198: 112388. https://doi.org/10.1016/j.eurpolymj.2023.112388

Lovati A B, D'Arrigo D, Odella S, Tos P, Geuna S, Raimondo S. Nerve repair using decellularized nerve grafts in rat models. A review of the literature. Frontiers in Cellular Neuroscience 2018; 12: 427. https://doi.org/10.3389/fncel.2018.00427

McInnes A D, Moser M A, Chen X. Preparation and use of decellularized extracellular matrix for tissue engineering. Journal of Functional Biomaterials 2022; 13: 240. https://doi.org/10.3390/jfb13040240

Moradi A, Ataollahi F, Sayar K, Pramanik S, Chong P P, Khalil A A, et al. Chondrogenic potential of physically treated bovine cartilage matrix derived porous scaffolds on human dermal fibroblast cells. Journal of Biomedical Materials Research Part A 2016; 104: 245-256. https://doi.org/10.1002/jbm.a.35561

Moreno-Manzano V, Mellado-López M, Morera-Esteve M J, Alastrue-Agudo A, Bisbal-Velasco V, Forteza-Vila J, et al. Human adipose-derived mesenchymal stem cells accelerate decellularized neobladder regeneration. Regenerative Biomaterials 2020; 7: 161-169. https://doi.org/10.1093/rb/rbz049

Philips C, Campos F, Roosens A, Sánchez-Quevedo M d C, Declercq H, Carriel V. Qualitative and quantitative evaluation of a novel detergent-based method for decellularization of peripheral nerves. Annals of Biomedical Engineering 2018; 46: 1921-1937. https://doi.org/10.1007/s10439-018-2082-y

Rosadas M, Silva I V, Costa J B, Ribeiro V P, Oliveira A L. Decellularized dermal matrices: unleashing the potential in tissue engineering and regenerative medicine. Frontiers in Materials 2024; 10: 1285948. https://doi.org/10.3389/fmats.2023.1285948

Sondell M, Lundborg G, Kanje M. Regeneration of the rat sciatic nerve into allografts made acellular through chemical extraction. Brain Research 1998; 795: 44-54. https://doi.org/10.1016/S0006-8993(98)00251-0

Sridharan R, Reilly R B, Buckley C T. Decellularized grafts with axially aligned channels for peripheral nerve regeneration. Journal of the Mechanical Behavior of Biomedical Materials 2015; 41: 124-135. https://doi.org/10.1016/j.jmbbm.2014.10.002

Sun Y, Zhang R, Mao X, Zhang M. Research of acellular xenogeneic nerve combined with adipose-derived stem cells and platelet rich plasma in repair of rabbit facial nerve injury. Zhongguo xiu fu Chong Jian wai ke za zhi= Zhongguo Xiufu Chongjian Waike Zazhi= Chinese Journal of Reparative and Reconstructive Surgery 2018; 32: 736-744.

Terenzio M, Koley S, Samra N, Rishal I, Zhao Q, Sahoo P K, et al. Locally translated mTOR controls axonal local translation in nerve injury. Science 2018; 359: 1416-1421. https://doi.org/10.1126/science.aan1053

Vijayavenkataraman S. Nerve guide conduits for peripheral nerve injury repair: A review on design, materials and fabrication methods. Acta Biomaterialia 2020; 106: 54-69. https://doi.org/10.1016/j.actbio.2020.02.003

Wang S, Liu X, Wang Y. Evaluation of platelet-rich plasma therapy for peripheral nerve regeneration: a critical review of literature. Frontiers in Bioengineering and Biotechnology 2022; 10: 808248. https://doi.org/10.3389/fbioe.2022.808248

Wong M L, Griffiths L G. Immunogenicity in xenogeneic scaffold generation: antigen removal vs. decellularization. Acta Biomaterialia 2014; 10: 1806-1816. https://doi.org/10.1016/j.actbio.2014.01.028

Yang X, Xue P, Chen H, Yuan M, Kang Y, Duscher D, et al. Denervation drives skeletal muscle atrophy and induces mitochondrial dysfunction, mitophagy and apoptosis via miR-142a-5p/MFN1 axis. Theranostics 2020; 10: 1415. https://doi.org/10.7150/thno.40857

Zaminy A, Sayad-Fathi S, Kasmaie F M, Jahromi Z, Zendedel A. Decellularized peripheral nerve grafts by a modified protocol for repair of rat sciatic nerve injury. Neural Regeneration Research 2021; 16: 1086-1092. https://doi.org/10.4103/1673-5374.300449

Zhang F, Zhang N, Xu Q, Zhang L, Zhang C, Liu H, et al. Decellularized nerve extracellular matrix/chitosan cross-linked by genipin to prepare a moldable nerve repair ma-

terial. Cell and Tissue Banking 2021; 22: 419-430. https://doi.org/10.1007/s10561-020-09889-2

Zilic L, Wilshaw S P, Haycock J W. Decellularisation and histological characterisation of porcine peripheral nerves. Biotechnology and Bioengineering 2016; 113: 2041-2053. https://doi.org/10.1002/bit.25964